Eur. Phys. J. C 45, 711–720 (2006)
Digital Object Identifier (DOI) 10.1140/epjc/s2005-02453-0

THE EUROPEAN
PHYSICAL JOURNAL C

Study of $B_c \to D\pi$ in the perturbative QCD approach

Jian-Feng Cheng[1,a], Dong-Sheng Du[2,3], Cai-Dian Lü[2,3]

[1] Institute of High Energy Physics, CAS, P.O. Box 918(4), Beijing 100049, China
[2] CCAST (World Laboratory), P.O. Box 8730, Beijing 100080, China
[3] Institute of High Energy Physics, CAS, P.O. Box 918(4), Beijing 100049, China[b]

Received: 22 September 2005 /
Published online: 5 January 2006 –

Abstract. We investigate the branching ratios and direct CP-asymmetries of the $B_c^+ \to D^0\pi^+$ and $B_c^+ \to D^+\pi^0$ decays in the PQCD approach. All the diagrams with emission topology or annihilation topology are calculated strictly. A branching ratio of 10^{-6} and 10^{-7} for $B_c^+ \to D^0\pi^+$ and $B_c^+ \to D^+\pi^0$ decay is predicted, respectively. Because of the different weak phase and strong phase from penguin operator and two kinds of tree operator contributions, we predict a possible large direct CP-violation: $A_{CP}^{\mathrm{dir}}(B_c^\pm \to D^0\pi^\pm) \approx -50\%$ and $A_{CP}^{\mathrm{dir}}(B_c^\pm \to D^\pm\pi^0) \approx 25\%$ when $\gamma = 55°$, which can be tested in the coming LHC.

PACS. 13.25.Hw, 12.38.Bx

1 Introduction

The charmless B decays provide a good platform to test the standard model (SM) and study the CP-violation, which arouses great interest and has been discussed in the literature widely. But how about the B_c decays, the b quark of which has properties similar to the B meson? There are some events of B_c at Tevatron [1] and there will be a great number of events appearing at LHC in the foreseeable future. The progress of the experiments leads us to think of the question: what will be the theoretical prediction on the two-body non-leptonic B_c decays?

Different from the B and B_s meson, the B_c meson consists of the two heavy quarks b and c, which can decay individually. Because of the difference of mass, lifetime and the relative CKM matrix element between b and c quark, the decay rate of the two quarks is different, which determines the unique property of B_c decays. Though the c quark's mass is about one third of the b quark, leading to a suppression of $(M_c/M_b)^5$, the decay of the c quark cannot be ignored because the corresponding CKM matrix element V_{cs} is larger than that of the b quark: V_{ub}, V_{cb}. Because of the small mass of the c quark, the decay of the c quark is nearly at the non-perturbative scale, where there is a great theoretical difficulty. Now we study the b quark decay first and leave the study of the c quark decay to the future.

In recent years, great progress has been made in studying two-body non-leptonic B decays in the perturbative QCD approach (PQCD) [2,3], QCD factorization [4] and soft collinear effective theory (SCET) [5]. Though B_c decay has been studied [6] in the naive factorization approach [7,8] many years ago, no one applies the method developed recently in such processes. In this paper we will use $B_c \to D\pi$ as an example to discuss the B_c decays in the PQCD approach.

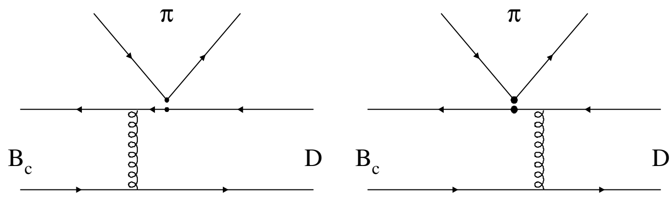

Fig. 1. Form factor in $B_c \to D\pi$

The $B_c \to D\pi$ decay provides opportunities to study the direct CP-asymmetry. Different from the B decays [3], $B_c \to D\pi$ has a direct CP-asymmetry even without considering the contributions from penguin operators, because the tree contributions from the annihilation topology provide not only the strong phase, but also the different weak phase. According to the power counting rule of PQCD, the tree contributions from the annihilation topology is power suppressed. But the larger CKM matrix elements $|V_{cb}|$ enhance the contribution making it larger than the penguin contributions, so the direct CP-asymmetry of $B_c \to D\pi$ can be very large, which is found in our numerical analysis.

The study of B_c decay also provides opportunities to test k_{T} factorization in the PQCD approach. According to the numerical analysis in the literature, the form factor contributions from Fig. 1 usually dominate the whole decay. In the same way, the form factor also gives the main contributions in the $B_c \to D\pi$ decay according to our numerical analysis. Since the B_c meson consists of two heavy

[a] e-mail: chengjf@mail.ihep.ac.cn
[b] Mailing address.

quarks, the effect of k_T in the B_c meson can be ignored and the form factor $B_c \to D$ only includes the k_T contributions from the D meson. So it is easier to study how important the k_T contributions are in B_c decays than in B decays because the latter need to consider both k_T contributions of B and D meson.

The $B_c \to D\pi$ decay also provides a good platform to study the D meson's wave function. The D meson's mass M_D is not so large that it is hard to get the ideal wave function of D meson by the expansion of $1/M_D$ as in the B meson. One uses the form fitted from experimental data generally. Such a discussion has been given by [9] in the form factor of the $B \to D$ transition. It is better to discuss the D meson wave function in $B_c \to D\pi$ for two reasons: one is that the hierarchy between M_{B_c} and M_D ($M_{B_c} \gg M_D$) guarantees us that we may apply the k_T factorization theorem in this process; the other one is that the wave function of B_c is clean, which eliminates the possible uncertainty from the B_c meson. The experiment of B_c decays will test how reasonable this is. As the only parameter with a large uncertainty, the wave function of D meson need further theoretical investigation.

2 Framework

The hard amplitudes of these decays contain factorizable diagrams (Fig. 1), where hard gluons attach the valence quarks in the same meson, and non-factorizable diagrams (Fig. 2), where hard gluons attach the valence quarks in different mesons. The annihilation topology is also included, and classified into factorizable (Fig. 3) and non-factorizable (Fig. 4) ones according to the above definitions.

In the calculations of all the diagrams, we can ignore the k_T contributions of B_c meson because it consists of two heavy quarks. Furthermore, we can suppose the two quarks $\bar{b}$ and c of B_c^+ meson to be on the mass shell approximately and treat the wave function of B_c meson as δ function for simplicity, so we can integrate the wave function B_c out

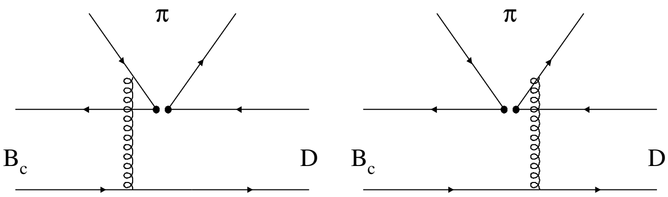

Fig. 2. Non-factorizable emission topology in $B_c \to D\pi$

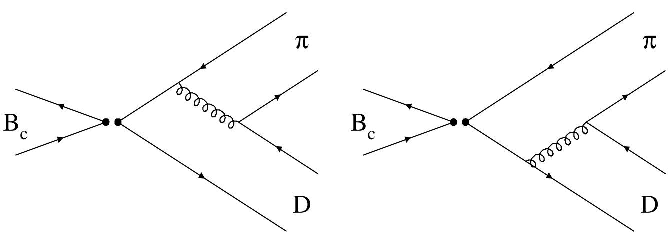

Fig. 3. Factorizable annihilation topology in $B_c \to D\pi$

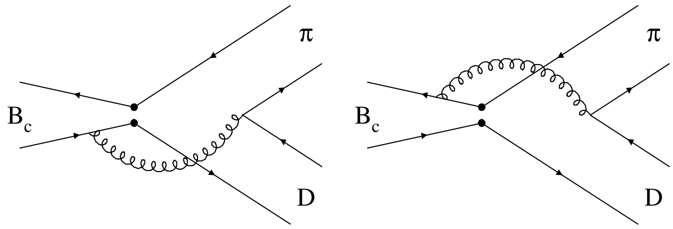

Fig. 4. Non-factorizable annihilation topology in $B_c \to D\pi$

and the k_T factorization form turns into

$$\text{Form factor} \tag{1}$$
$$\sim \int \mathrm{d}^4 k_1\, \Phi_D(k_1)\, C(t)\, H(k_1,t),$$
$$\text{Other topology} \tag{2}$$
$$\sim \int \mathrm{d}^4 k_1 \mathrm{d}^4 k_2\, \Phi_D(k_1) \Phi_\pi(k_2)\, C(t)\, H(k_1,k_2,t),$$

where $k_{1(2)}$ is the momentum of the light (anti-) quark of the $D(\pi)$ meson. The non-factorizable topology includes two kinds of topology: the emission topology (Fig. 2) and the annihilation topology (Fig. 4). In the above equations, we sum over all Dirac structure and color indices. The hard components consist of the hard part ($H(t)$) and the harder dynamics ($C(t)$). The former $H(t)$ can be calculated perturbatively; the latter $C(t)$ is for the Wilson coefficients which run from the electroweak scale M_W to the lower factorization scale t. Φ_M is the wave function of the D and π meson, including the non-perturbative contributions in the k_T factorization.

Throughout this paper, we use the light-cone coordinate to describe the meson's momentum in the rest frame of the B_c meson. According to the conservation of four-momentum, we get the momentum of the three mesons B_c, D and π up to the order of r_2^2 ($r_2 = M_D/M_{B_c}$) as follows:

$$P_{B_c} = \frac{M_{B_c}}{\sqrt{2}}(1,1,\mathbf{0}_\mathrm{T}),$$
$$P_2 = \frac{M_{B_c}}{\sqrt{2}}(1,r_2^2,\mathbf{0}_\mathrm{T}),$$
$$P_3 = \frac{M_{B_c}}{\sqrt{2}}(0,1-r_2^2,\mathbf{0}_\mathrm{T}), \tag{3}$$

where we have neglected the small mass of the pion and higher order terms of r_2. Such an approximation will be used in the whole paper.

3 Calculation of amplitudes

3.1 Wave function

The B_c meson consists of two heavy quarks such that the small $\bar{\Lambda}_\mathrm{QCD}$ can be ignored ($\bar{\Lambda}_\mathrm{QCD} = M_{B_c} - M_b - M_c \ll M_c$ or M_b), as can the quark transverse momentum k_T. In principle there are two Lorentz structures in the B or B_c

meson wave function. One should consider both of them in calculations. However, it can be argued that one of the contributions is numerically small [10], thus its contribution can be neglected. Therefore, we only consider the contribution of one Lorentz structure, such that we can reduce the number of input parameters:

$$\Phi_{B_c}(x) = \frac{\mathrm{i}}{4N_c}(\not{p}_{B_c} + M_{B_c})\,\gamma_5\,\delta(x - M_c/M_{B_c}). \quad (4)$$

The other two mesons' wave functions read

$$\Phi_D(x,b) = \frac{\mathrm{i}}{\sqrt{2N_c}}\gamma_5(\not{P}_2 + M_D)\phi_D(x,b), \quad (5)$$

$$\Phi_\pi(x) = \frac{\mathrm{i}}{\sqrt{2N_c}}\left[\gamma_5\ \not{P}_3\phi_\pi(x) + M_{0\pi}\gamma_5\phi_\pi^p(x) + M_{0\pi}\gamma_5(\not{n}_-\not{n}_+ - 1)\phi_\pi^\sigma(x)\right], \quad (6)$$

where $N_c = 3$ is color degree of freedom, and $M_{0\pi} = M_\pi^2/(m_u + m_d)$, $n_- = (0,1,\mathbf{0}_\mathrm{T}) \propto P_3$, $n_+ = (1,0,\mathbf{0}_\mathrm{T})$, $\epsilon^{0123} = 1$.

The momentum fraction of the light quark in the three mesons can be defined by $x_1 = k_c/P_{B_c}, x_2 = k_2^+/P_2^+, x_3 = k_3^-/P_3^-$. In the B_c meson, there is also another relation between x_1 and $r_b = M_b/M_{B_c}$: $x_1 + r_b = 1$.

3.2 Effective Hamiltonian

The effective Hamiltonian for the flavor-changing $b \to d$ transition is given by [11]

$$H_\mathrm{eff} = \frac{G_\mathrm{F}}{\sqrt{2}}\sum_{q=u,c} V_q\left[C_1(\mu)O_1^{(q)}(\mu) + C_2(\mu)O_2^{(q)}(\mu) + \sum_{i=3}^{10} C_i(\mu)O_i(\mu)\right], \quad (7)$$

with the Cabibbo–Kobayashi–Maskawa (CKM) matrix elements $V_q = V_{qd}V_{qb}^*$ and the operators

$$\begin{aligned}
O_1^{(q)} &= (\bar{d}_i q_j)_{V-A}(\bar{q}_j b_i)_{V-A},\\
O_2^{(q)} &= (\bar{d}_i q_i)_{V-A}(\bar{q}_j b_j)_{V-A},\\
O_3 &= (\bar{d}_i b_i)_{V-A}\sum_q(\bar{q}_j q_j)_{V-A},\\
O_4 &= (\bar{d}_i b_j)_{V-A}\sum_q(\bar{q}_j q_i)_{V-A},\\
O_5 &= (\bar{d}_i b_i)_{V-A}\sum_q(\bar{q}_j q_j)_{V+A},\\
O_6 &= (\bar{d}_i b_j)_{V-A}\sum_q(\bar{q}_j q_i)_{V+A},\\
O_7 &= \frac{3}{2}(\bar{d}_i b_i)_{V-A}\sum_q e_q(\bar{q}_j q_j)_{V+A},\\
O_8 &= \frac{3}{2}(\bar{d}_i b_j)_{V-A}\sum_q e_q(\bar{q}_j q_i)_{V+A},\\
O_9 &= \frac{3}{2}(\bar{d}_i b_i)_{V-A}\sum_q e_q(\bar{q}_j q_j)_{V-A},\\
O_{10} &= \frac{3}{2}(\bar{d}_i b_j)_{V-A}\sum_q e_q(\bar{q}_j q_i)_{V-A},
\end{aligned} \quad (8)$$

with i and j being the color indices. Using the unitary condition, the CKM matrix elements for the penguin operators O_3–O_{10} can also be expressed as $V_u + V_c = -V_t$.

The $B_c \to D\pi$ decay rates have the expressions

$$\Gamma = \frac{G_\mathrm{F}^2 M_{B_c}^3}{32\pi}|A|^2. \quad (9)$$

The decay amplitude A of the $B_c \to D\pi$ process from all the diagrams can be expressed as follows:

$$\begin{aligned}
A_{D^0\pi^+} &= V_u\left(f_\pi F_\mathrm{e1}^\mathrm{T} + M_\mathrm{e1}^\mathrm{T}\right) + V_c\left(f_{B_c}F_\mathrm{a}^\mathrm{T} + M_\mathrm{a}^\mathrm{T}\right)\\
&\quad - V_t\left(f_\pi F_\mathrm{e1}^\mathrm{P1} + f_\pi F_\mathrm{e1}^\mathrm{P3} + M_\mathrm{e1}^\mathrm{P1} + M_\mathrm{e1}^\mathrm{P2}\right. \quad (10)\\
&\quad \left. + f_{B_c}F_\mathrm{a}^\mathrm{P1} + f_{B_c}F_\mathrm{a}^\mathrm{P3} + M_\mathrm{a}^\mathrm{P1} + M_\mathrm{a}^\mathrm{P2}\right),\\
\sqrt{2}A_{D^+\pi^0} &= V_u\left(f_\pi F_\mathrm{e2}^\mathrm{T} + M_\mathrm{e2}^\mathrm{T}\right) - V_c\left(f_{B_c}F_\mathrm{a}^\mathrm{T} + M_\mathrm{a}^\mathrm{T}\right)\\
&\quad - V_t\left(f_\pi F_\mathrm{e2}^\mathrm{P1} + f_\pi F_\mathrm{e2}^\mathrm{P2} + f_\pi F_\mathrm{e2}^\mathrm{P3}\right.\\
&\quad + M_\mathrm{e2}^\mathrm{P1} + M_\mathrm{e2}^\mathrm{P2} + M_\mathrm{e2}^\mathrm{P3} - f_{B_c}F_\mathrm{a}^\mathrm{P1}\\
&\quad \left. - f_{B_c}F_\mathrm{a}^\mathrm{P3} - M_\mathrm{a}^\mathrm{P1} - M_\mathrm{a}^\mathrm{P2}\right), \quad (11)
\end{aligned}$$

where $F(\mathcal{M})$ denotes factorizable (non-factorizable) amplitudes, the subscript e(a) denotes the emission (annihilation) diagrams. The subscript 1(2) denotes the process $B_c^+ \to D^0\pi^+$ ($B_c^+ \to D^+\pi^0$), the superscript T(P) denotes amplitudes from the tree (penguin) operators, and f_{B_c} (f_π) is the B_c (π) meson decay constant. The detailed expressions of these amplitudes are shown in Appendix A.

From (10) and (11), we can see that unlike $B^\pm$, $B^0(\bar{B}^0)$ decays, we have three kinds of decay amplitudes with different weak and strong phases: penguin contributions proportional to V_t and two kinds of tree contributions proportional to V_c and V_u, respectively. The interference between them gives a large direct CP-violation which will be shown later.

As stated in the introduction, the two diagrams in Fig. 1 give the contribution for the $B_c \to D$ transition form factor, which is defined by

$$\langle D|d\gamma^\mu b|B_c\rangle = F_+\left(p_{B_c}^\mu + p_D^\mu\right) + F_-\left(p_{B_c}^\mu - p_D^\mu\right). \quad (12)$$

We calculate F_+ in PQCD and get

$$\begin{aligned}
F_+ = {} & \frac{4f_B}{\sqrt{2N_c}}\pi C_F M_{B_c}^2\int_0^1 \mathrm{d}x_2\int_0^\infty b_2\mathrm{d}b_2\,\phi_D(x_2,b_2)\\
&\times\Big\{\left[2r_b - x_2 - (r_b - 2x_2)r_2 + (x_2 - 2r_b)r_2^2\right]\\
&\times\alpha_\mathrm{s}\left(t_\mathrm{e}^{(1)}\right)S_D\left(t_\mathrm{e}^{(1)}\right)H_\mathrm{e1}\left(\alpha_\mathrm{e},\beta_\mathrm{e1},b_2\right)\\
&+\left[(1 - x_1)r_2(2 - r_2)\right]
\end{aligned}$$

Table 1. Form factor F_+ in the different values of ω_D

ω_D	0.40 GeV	0.45 GeV	0.50 GeV
F_+	0.154	0.169	0.174

$$\times\alpha_s\left(t_e^{(2)}\right) S_D\left(t_e^{(2)}\right) H_{e2}\left(\alpha_e,\beta_{e2},b_2\right)\Big\}, \qquad (13)$$

which is an expression similar to F_{e1}^{T} without Wilson coefficients in the appendix. The numerical results of F_+ can be found in Table 1: the form factor F_+ is $0.169^{+0.05}_{-0.15}$ including the uncertainty of ω_D, which is comparable with previous calculations [6, 12].

3.3 Input parameters

For the D meson wave function, two types of D meson wave function are usually used in the literature: one is [9]

$$\phi_D(x) = \frac{3}{\sqrt{2N_c}} f_D x(1-x)\{1+a_D(1-2x)\} \times \exp\left[-\frac{1}{2}\left(\omega_D b\right)^2\right], \qquad (14)$$

in which the last term, $\exp\left[-\frac{1}{2}\left(\omega_D b\right)^2\right]$, represents the k_T distribution; the other one [13, 14] is

$$\phi_D(x) = \frac{3}{\sqrt{2N_c}} f_D x(1-x)\{1+a_D(1-2x)\}, \qquad (15)$$

which is fitted from the measured $B \to D\ell\nu$ decay spectrum at large recoil. The absence of the last term in the (14) is due to the insufficiency of the experimental data.

Though the wave function of the D meson turns out to be more complicated when it runs at a velocity of about $0.6c$, the light quark's momentum must be less than $p_2^+/2$ because the mass of the c quark is by far larger than Λ_{QCD}: $M_c \gg \Lambda_{QCD}$, so the wave function of D meson should be strongly suppressed in the region $x_2 > 1/2$ and even the k_T contributions are considered. In order to satisfy the above condition, we give up the D wave functions above and construct a new wave function, which also fits the measured $B \to Dl\nu$ decay spectrum at large recoil:

$$\phi_D(x,b) = N_D\left[x(1-x)\right]^2 \times \exp\left[-\frac{1}{2}\left(\frac{xM_D}{\omega_D}\right)^2 - \frac{1}{2}\left(\omega_D\right)^2 b^2\right], \qquad (16)$$

where N_D is a normalization constant to let

$$\int_0^1 \phi_D(x,b) = \frac{f_D}{2\sqrt{2N_c}}. \qquad (17)$$

The behavior of the whole D meson wave function can be seen in Fig. 5. Our choice of the third case has a broad peak at the small x side, which characterizes the mass difference of m_c and m_d.

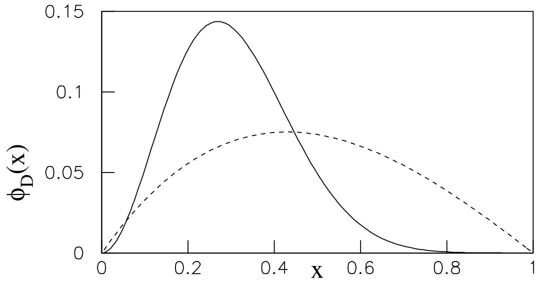

Fig. 5. D meson wave functions: the dashed line for case 1 and 2, the solid line for case 3

The π wave functions [15, 16] we adopt are calculated by QCD sum rules and shown in Appendix B.

The other input parameters are listed below [17, 18]:

$$\begin{aligned} f_{B_c} &= 480\,\text{MeV}, \quad f_D = 240\,\text{MeV}, \quad f_\pi = 131\,\text{MeV}, \\ \omega_D &= 0.45\,\text{GeV}, \quad M_{0\pi} = 1.60\,\text{GeV}, \quad a_D = 0.3, \\ M_{B_c} &= 6.4\,\text{GeV}, \quad M_b = 4.8\,\text{GeV}, \\ M_D &= 1.869\,\text{GeV}, \quad M_t = 170\,\text{GeV}, \\ M_W &= 80.4\,\text{GeV}, \quad \tau_{B^\pm} = 0.46\times10^{-12}\,\text{s}, \\ G_F &= 1.16639\times10^{-5}\,\text{GeV}^{-2}. \end{aligned} \qquad (18)$$

The CKM parameters used in the paper are

$$\left|\frac{V_{ub}}{V_{cb}}\right| = 0.085 \pm 0.020, \qquad (19)$$

$$|V_{cb}| = 0.039 \pm 0.002, \qquad (20)$$

$$R = \left|\frac{V_u}{V_c}\right| = \frac{1-\lambda^2/2}{\lambda}\left|\frac{V_{ub}}{V_{cb}}\right|. \qquad (21)$$

The CKM angle $\phi_3 = \gamma$ is left as a free parameter to discuss CP-violation, defined by

$$\gamma = \arg\left(-\frac{V_u}{V_c}\right) = \arg\left(V_{ub}^*\right). \qquad (22)$$

3.4 Numerical analysis

We fix $\gamma = 55°$ to discuss the central value of the numerical results first.

Both process $B_c^+ \to D^0\pi^+$ and $B_c^+ \to D^+\pi^0$ are tree-dominated. The branching ratios and main contributions are give in Table 2, from which we can see that the branching ratio of $B_c^+ \to D^0\pi^+$ is much larger than that of $B_c^+ \to D^+\pi^0$. Though they are both a tree-dominated process, their branching ratios and percentage of different topologies in the whole process are obviously different. Because the annihilation topology gives the same contributions to both processes, despite a $\sqrt{2}$ factor, the difference only comes from the emission topology. In the process $B_c^+ \to D^0\pi^+$, contributions from the factorizable emission topology dominate the whole tree contributions for the large Wilson coefficients $C_2 + C_1/N_c$ in (A.13), which occupy about 93% of the total even when the effect of CKM

Table 2. Branch ratios and main contributions from tree operators (10^{-3} GeV)

	$B_c^+ \to D^0\pi^+$	$B_c^+ \to D^+\pi^0$
$f_\pi F_{\mathrm{e}}^{\mathrm{T}}$	23.0	0.763
$M_{\mathrm{e}}^{\mathrm{T}}$	$-0.379 + 0.863\mathrm{i}$	$0.854 - 2.16\mathrm{i}$
$f_B F_{\mathrm{a}}^{\mathrm{T}}$	$-3.35 + 5.49\mathrm{i}$	$-3.35 + 5.49\mathrm{i}$
$M_{\mathrm{a}}^{\mathrm{T}}$	$2.52 - 1.92\mathrm{i}$	$2.52 - 1.92\mathrm{i}$
$\left\lvert \frac{P}{T_{\mathrm{e}}} \right\rvert$	10%	40%
Br	0.978×10^{-6}	0.196×10^{-6}

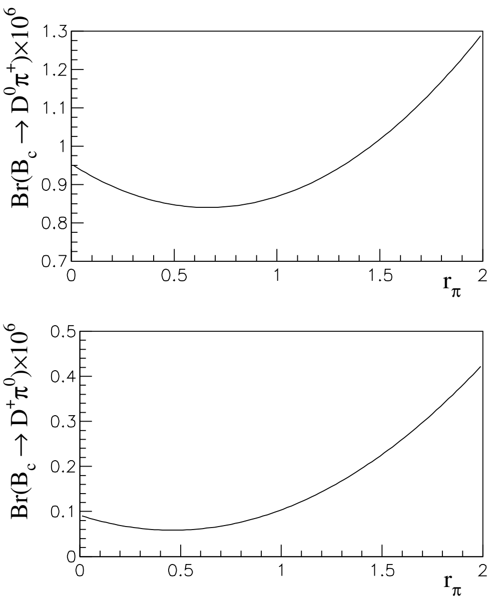

Fig. 6. The correlation between $\mathrm{Br}(B_c \to D\pi)$ and r_π

matrix element is considered ($|\lambda_u| < |\lambda_c|$). On the contrary, contributions from the factorizable emission topology in the process $B_c^+ \to D^+\pi^0$ are suppressed because the Wilson coefficients C_1 and C_2/N_c in (A.14) cancel each other approximately. From Table 2 we also find that contributions from the factorizable annihilation topology are at the same order of non-factorizable emission topology.

The ratio of the penguin contributions over the tree contributions is about 10% in the process $B_c^+ \to D^0\pi^+$ and about 40% in the process $B_c^+ \to D^+\pi^0$ (Table 2). The reason for the difference is the term $2r_\pi\phi_\pi^p(x_3)$ in (A.4) from the O_6, O_8 operator contributions, having no factors like x_3 to suppress its integral value in the end-point region and leading to large enhancement compared with other penguin contributions. But the most important reason is that the tree contribution is suppressed in the process $B_c^+ \to D^+\pi^0$ due to the small Wilson coefficients $C_1 + C_2/3$ but is not suppressed in the process $B_c^+ \to D^0\pi^+$. The O_6, O_8 contributions also affect the dependence behavior of the branching ratio and the direct CP-asymmetry on the CKM angle γ in the process $B_c^\pm \to D^\pm\pi^0$, which will be discussed in the following.

The correlation between $\mathrm{Br}(B_c^+ \to D\pi)$ and r_π is shown in Fig. 6. Because twist-3 terms of the π wave function do not contribute to the form factor ((A.1) and (A.2)), the variation of r_π affects the process $B_c^+ \to D^+\pi^0$ more heavily than the process $B_c^+ \to D^0\pi^+$, where the latter dominated by the $B_c \to D$ form factor diagrams. When $r_\pi = 1.4$, the twist-3 contributions are about 25% in the process $B_c^+ \to D^0\pi^+$. In the process $B_c^+ \to D^+\pi^0$, the twist-3 contributions with a relative minus sign cancel some of the twist-2 contributions. When $r_\pi = 1.4$, the branching ratio of $B_c^+ \to D^+\pi^0$ is about four times the branching ratio with only twist-2 contributions. When $r_\pi = 0$, the twist-3 contributions vanish and only the contributions from twist-2 terms in the π wave function are left. The corresponding branching ratio is reduced to 0.95×10^{-6} in the process $B_c^+ \to D^0\pi^+$ and 0.092×10^{-6} in the process $B_c^+ \to D^+\pi^0$ respectively.

Table 3. Branch ratios in the unit 10^{-6} for different ω_D

	$B_c^+ \to D^0\pi^+$	$B_c^+ \to D^+\pi^0$
$\omega_D = 0.40\,\mathrm{GeV}$	1.03	0.128
$\omega_D = 0.45\,\mathrm{GeV}$	0.978	0.196
$\omega_D = 0.50\,\mathrm{GeV}$	1.19	0.199

As the only free parameter with a large uncertainty, the value of ω_D is the key point to the whole prediction in the calculations of $B_c \to D\pi$. In Table 3 we discuss the branching ratio in three groups of different ω values: $\omega_D = 0.40\,\mathrm{GeV}$, $\omega_D = 0.45\,\mathrm{GeV}$ and $\omega_D = 0.50\,\mathrm{GeV}$, from which we see that the variation of ω_D affects the process $B_c^+ \to D^0\pi^+$ slightly, but affects the process $B_c^+ \to D^+\pi^0$ heavily.

According to the CKM parametrization shown in (19)–(22), the decay amplitudes of $B_c \to D\pi$ can be written as

$$\begin{aligned} M_{D\pi} &= V_u T_u + V_c T_c - V_t P \\ &= V_u (T_u + P)\left[1 - \frac{1}{R}\frac{T_c + P}{T_u + P}\mathrm{e}^{-\mathrm{i}\gamma}\right] \\ &\equiv V_u (T_u + P)\left[1 - z\mathrm{e}^{\mathrm{i}(-\gamma+\delta)}\right], \end{aligned} \qquad (23)$$

where $z = \frac{1}{R}\left|\frac{T_c+P}{T_u+P}\right| = \left|\frac{V_c}{V_u}\right|\left|\frac{T_c+P}{T_u+P}\right|$ and the strong phase $\delta = \arg\left(T_c + \frac{P}{T_u} + P\right)$, from our PQCD calculation the numerical value of which is 0.28 and 123° for $B_c^+ \to D^0\pi^+$, respectively. The emission topology in this channel is only about one time larger than the annihilation topology due to the small CKM factor $|V_u/V_c|$.

The corresponding conjugate decay of $B_c^+ \to D\pi$ reads

$$M_{B_c^- \to \bar{D}\pi^{-(0)}} = V_u^*(T_u + P)\left[1 - z\mathrm{e}^{\mathrm{i}(\gamma+\delta)}\right], \qquad (24)$$

and the averaged branching ratio for $B_c^\pm \to D^0(\bar{D}^0)\pi^\pm$ reads

$$\begin{aligned} \mathrm{Br} &= \frac{1}{2}(|M|^2 + |\bar{M}|^2) \\ &= \frac{1}{2}|V_u(T_u + P)|^2\left[1 - 2z\cos\gamma\cos\delta + z^2\right], \end{aligned} \qquad (25)$$

which is a function of the CKM angle γ. Its numerical result depends on γ significantly: the larger γ, the smaller the

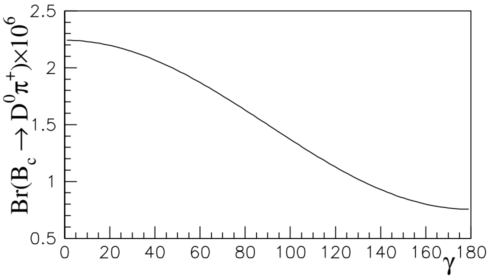

Fig. 7. The correlation between the averaged branching ratio and γ in the process $B_c^\pm \to D^0\pi^\pm$

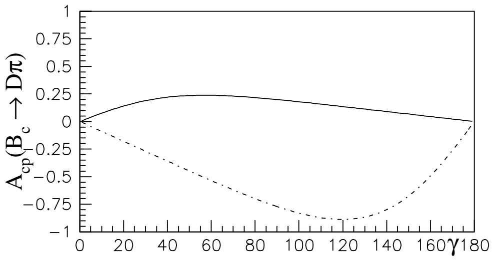

Fig. 8. The correlation between the direct CP-violation and γ, the solid line for $B_c^\pm \to D^\pm\pi^0$ and the dashed line for $B_c^\pm \to D^0(\bar{D}^0)\pi^\pm$

averaged branching ratio, because $\cos\delta < 0$. The explicit correlation between the averaged branching ratio $B_c^\pm \to D^0(\bar{D}^0)\pi^\pm$ and γ is shown in Fig. 7.

The direct CP-violation A_{CP}^{dir} is defined as

$$A_{CP}^{\mathrm{dir}} = \frac{\left|M(B_c^+ \to D^{0(+)}\pi^{+(0)}\right|^2 - \left|M(B_c^- \to D^{0(-)}\pi^{-(0)}\right|^2}{\left|M(B_c^+ \to D^{0(+)}\pi^{+(0)}\right|^2 + \left|M(B_c^- \to D^{0(-)}\pi^{-(0)}\right|^2}. \tag{26}$$

There are two different tree contributions and one kind of penguin contribution with different strong and weak phases, which will contribute to the CP-asymmetry. Using (23) and (24), A_{CP}^{dir} can be simplified as

$$A_{CP}^{\mathrm{dir}} = -\frac{2z\sin\delta\sin\gamma}{1 - 2z\cos\delta\cos\gamma + z^2}, \tag{27}$$

which is proportional to $\sin\gamma$ approximately. This is shown in Fig. 8. When $\gamma = 55°$, the direct CP-asymmetry is about -50% in the process $B_c^+ \to D^0\pi^+$.

The $B_c \to D^+\pi^0$ process becomes a little more complicated: the tree contributions from the emission topology $M_{\mathrm{e}}^{\mathrm{T}}$ (in Table 1) is suppressed due to the small Wilson coefficients $C_1 + C_2/3$. In this case, the three different contributions with different weak and strong phases (two tree contributions and one penguin contribution) are at the same order of magnitude. We can still use (25) and (27) to get the behavior of the branching ratio and the direct CP-asymmetry on γ. Now the numerical values of z and δ are 3.1 and $-20°$ respectively. Different from the averaged branching ratio of the process $B_c \to D^+\pi^0$, the averaged branching ratio of the process $B_c \to D^0\pi^+$ becomes smaller when γ becomes larger because $\cos\delta > 0$.

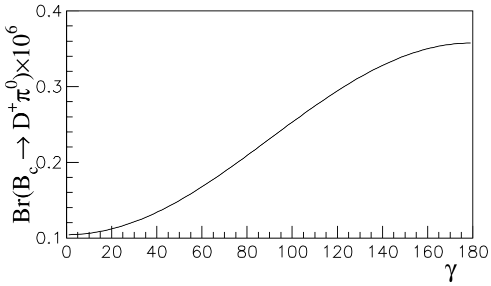

Fig. 9. The correlation between the averaged branching ratio and γ in the process $B_c^\pm \to D^\pm\pi^0$

The behavior of the branching ratio and the direct CP-asymmetry does not change much, but the shape of the former turns sharper. In one word, the branching ratios of $B_c^\pm \to D^\pm\pi^0$ shown in Fig. 9 are more sensitive to the value of γ, which is quite different from the case for $B_c^\pm \to D^0\pi^\pm$, but the direct CP-asymmetry of $B_c^\pm \to D^\pm\pi^0$ shown in Fig. 8 does not change greatly because the large uncertainty from γ cancels in the ratio of the direct CP-asymmetry. When $\gamma = 55°$, the direct CP-asymmetry is about 25% in the process $B_c^\pm \to D^\pm\pi^0$. As pointed out in [19], the CP-asymmetry is sensitive to the next-to-leading order contribution, which is more complicated; the result shown here should be taken carefully.

4 Conclusion

In this paper we discuss the process $B_c \to D^0\pi^+$ and $B_c \to D^+\pi^0$ in the PQCD approach and get their branching ratios $1.03^{+0.16}_{-0.04} \times 10^{-6}$ and $1.96^{+0.03}_{-0.68} \times 10^{-7}$ respectively. We also predict the possible large direct CP-asymmetry in the two processes $A_{CP}^{\mathrm{dir}}(B_c^\pm \to D^0\pi^\pm) \approx -50\%$ and $A_{CP}^{\mathrm{dir}}(B_c^\pm \to D^\pm\pi^0) \approx 25\%$ when $\gamma = 55°$. The possible theoretical uncertainty is also analyzed. We hope it can be tested in the coming experiments at Tevatron, LHC and the super-B factory.

Acknowledgements. One of the authors (JFC) thanks C.H. Chang, Y. Li, Y.-L. Shen and X.-Q. Yu for the beneficial discussions. This work is partly supported by National Science Foundation of China.

Appendix A: Contributions from all diagrams

1. Contributions from factorizable diagrams

All diagrams are sorted into two kinds: emission topology and annihilation topology shown in Figs. 1 and 3, and Fig. 2 and 4. The factorizable tree contributions from emission topology read

$$F_{ei}^{\mathrm{T(P1,P2)}} = \frac{4f_B}{\sqrt{2N_c}}\pi C_F M_{B_c}^2 \int_0^1 \mathrm{d}x_2 \int_0^\infty b_2 \mathrm{d}b_2\, \phi_D(x_2, b_2)$$

$$\times\Big\{\left[2r_b - x_2 - (r_b - 2x_2)r_2 + (x_2 - 2r_b)r_2^2\right]$$
$$\times E_{ei}^{\mathrm{T(P1,P2)}}(t_{\mathrm{e}}^{(1)})H_{\mathrm{e1}}(\alpha_{\mathrm{e}}, \beta_{\mathrm{e1}}, b_2)$$
$$+[(1-x_1)r_2(2-r_2)]$$
$$\times E_{ei}^{\mathrm{T(P1,P2)}}(t_{\mathrm{e}}^{(2)})H_{\mathrm{e2}}(\alpha_{\mathrm{e}}, \beta_{\mathrm{e2}}, b_2)\Big\}, \quad (A.1)$$

$$F_{ei}^{\mathrm{P3}}$$
$$= -\frac{8f_B}{\sqrt{2N_c}} r_K \pi C_F M_{B_c}^2 \int_0^1 \mathrm{d}x_2 \int_0^\infty b_2 \mathrm{d}b_2\, \phi_D(x_2, b_2)$$
$$\times\Big\{\left[-2 + r_b + (1 - 4r_b + x_2)r_2 + (r_b - 2x_2 + 2)r_2^2\right]$$
$$\times E_{ei}^{\mathrm{P3}}(t_{\mathrm{e}}^{(1)})H_{\mathrm{e1}}(\alpha_{\mathrm{e}}, \beta_{\mathrm{e1}}, b_2)$$
$$-\left[x_1 + 2(1-2x_1)r_2 - (2-x_1)r_2^2\right]$$
$$\times E_{ei}^{\mathrm{P3}}(t_{\mathrm{e}}^{(2)})H_{\mathrm{e2}}(\alpha_{\mathrm{e}}, \beta_{\mathrm{e2}}, b_2)\Big\}. \quad (A.2)$$

Because b and c are both massive quarks, there is no collinear divergence in the $B_c \to D$ transition, so the threshold resummation need not be considered. In all the expressions, T denotes the contributions from tree operators, P1 denotes the penguin contributions with the Dirac structure $(V-A)\otimes(V-A)$, P2 denotes the penguin contributions with the Dirac structure $(V-A)\otimes(V+A)$, and P3 denotes the penguin contributions with the Dirac structure $(S-P)\otimes(S+P)$; the subscript e(a) denotes the factorizable emission (annihilation) diagrams, the subscript n (na) denotes the non-factorizable emission (annihilation) diagrams.

The factorizable tree contributions from the annihilation topology read

$$F_a^{\mathrm{T(P1)}}$$
$$= 8\pi C_F M_{B_c}^2 \int_0^1 \mathrm{d}x_2 \mathrm{d}x_3 \int_0^\infty b_2 \mathrm{d}b_2 b_3 \mathrm{d}b_3\, \phi_D(x_2, b_2)$$
$$\times\Big\{\left[\left(x_3 - (1+2x_3)r_2^2\right)\phi_\pi(x_3)\right.$$
$$\left.+r_2 r_\pi\left((1+2x_3)\phi_\pi^p(x_3) - (1-2x_3)\phi_\pi^\sigma(x_3)\right)\right]$$
$$\times E_a^{\mathrm{T(P1)}}(t_{\mathrm{a}}^{(1)})H_{\mathrm{a}}(\alpha_{\mathrm{a}}, \beta_{\mathrm{a1}}, b_2, b_3)S_t(x_3)$$
$$-\left[x_2(1-r_2^2)\phi_\pi(x_3) + 2r_2 r_\pi(1+x_2)\phi_\pi^p(x_3)\right]$$
$$\times E_a^{\mathrm{T(P1)}}(t_{\mathrm{a}}^{(2)})H_{\mathrm{a}}(\alpha_{\mathrm{a}}, \beta_{\mathrm{a2}}, b_3, b_2)S_t(x_2)\Big\}, \quad (A.3)$$

$$F_a^{\mathrm{P3}}$$
$$= -16\pi C_F M_{B_c}^2 \int_0^1 \mathrm{d}x_2 \mathrm{d}x_3 \int_0^\infty b_2 \mathrm{d}b_2 b_3 \mathrm{d}b_3\, \phi_D(x_2, b_2)$$
$$\times\Big\{\left[-r_2\phi_\pi(x_3) + r_\pi\left(-x_3 + (2+x_3)r_2^2\right)\phi_\pi^p\right.$$
$$\left.+r_\pi x_3(1-r_2^2)\phi_\pi^\sigma(x_3)\right]$$
$$\times E_a^{\mathrm{P3}}(t_{\mathrm{a}}^{(1)})H_{\mathrm{a}}(\alpha_{\mathrm{a}}, \beta_{\mathrm{a2}}, b_2, b_3)S_t(x_3)$$
$$-\left[x_2 r_2\phi_\pi(x_3) + 2r_\pi\left(1 - (1-x_2)r_2^2\right)\phi_\pi^p(x_3)\right]$$
$$\times E_a^{\mathrm{P3}}(t_{\mathrm{a}}^{(2)})H_{\mathrm{a}}(\alpha_{\mathrm{a}}, \beta_{\mathrm{a2}}, b_3, b_2)S_t(x_2)\Big\}, \quad (A.4)$$

where the factor $S_t(x)$ is the jet function from the threshold resummation [20]

$$S_t(x) = \frac{2^{1+2c}\Gamma(3/2+c)}{\sqrt{\pi}\Gamma(1+c)}[x(1-x)]^c, \quad c = 0.3. \quad (A.5)$$

The factors $E_i^{T(P)}(t)$ contain the Wilson coefficients $a(t)$ at scale t and the evolution from t to the factorization scale $1/b$ in the Sudakov factors $S(t)$:

$$E_{ej}^{\mathrm{T(P}i)}(t) = \alpha_{\mathrm{s}}(t)a_{ej}^{\mathrm{T(P}i)}(t)\, S_D(t),$$
$$E_a^{\mathrm{T(P}i)}(t) = \alpha_{\mathrm{s}}(t)a_{\mathrm{e1}}^{\mathrm{T(P}i)}(t)\, S_D(t)S_\pi(t), \quad (A.6)$$

where $S_D(t), S_\pi(t)$, the Sudakov factors, are defined as

$$S_D(t) = s(x_2P_2^+, b_2) + 2\int_{1/b_2}^t \frac{\mathrm{d}\mu}{\mu}\gamma_q(\mu), \quad (A.7)$$
$$S_\pi(t) = s(x_3P_3^-, b_3) + s((1-x_3)P_3^-, b_3)$$
$$+2\int_{1/b_3}^t \frac{\mathrm{d}\mu}{\mu}\gamma_q(\mu), \quad (A.8)$$

and $s(Q,b)$ is given by [21]

$$s(Q,b) \quad (A.9)$$
$$= \int_{1/b}^Q \frac{\mathrm{d}\mu}{\mu}\left[\left\{\frac{2}{3}(2\gamma_{\mathrm{E}} - 1 - \ln 2) + C_F \ln\frac{Q}{\mu}\right\}\frac{\alpha_{\mathrm{s}}(\mu)}{\pi}\right.$$
$$\left.+\left\{\frac{67}{9} - \frac{\pi^2}{3} - \frac{10}{27}n_f + \frac{2}{3}\beta_0 \ln\frac{\mathrm{e}^{\gamma_{\mathrm{E}}}}{2}\right\}\left(\frac{\alpha_{\mathrm{s}}(\mu)}{\pi}\right)^2 \ln\frac{Q}{\mu}\right],$$

where the Euler constant $\gamma_{\mathrm{E}} = 0.57722\ldots$, and $\gamma_q = -\alpha_{\mathrm{s}}/\pi$ is the quark anomalous dimension.

The hard functions H are

$$H_{\mathrm{e1}}(\alpha, \beta, b) = \frac{K_0(\alpha b) - K_0(\beta b)}{\beta^2 - \alpha^2}, \quad (A.10)$$
$$H_{\mathrm{e2}}(\alpha, \beta, b) = \frac{1}{(1-x_1)(x_1 - r_2^2)}K_0(\alpha b), \quad (A.11)$$
$$H_{\mathrm{a}}(\alpha, \beta, b_1, b_2)$$
$$= [\theta(b_1 - b_2)K_0(\alpha b_1)I_0(\alpha b_2) \quad (A.12)$$
$$+\theta(b_2 - b_1)K_0(\alpha b_2)I_0(\alpha b_1)]\, K_0(\beta b_2),$$

where K_0, I_0, H_0 and J_0 are the Bessel functions of order 0. It is implied that the transformed Bessel functions K_0 and I_0 become the corresponding Bessel functions with real variable when their variables are complex.

The Wilson coefficients a_i read

$$a_{\mathrm{e1}}^{\mathrm{T}}(t) = C_2 + \frac{C_1}{N_c}, \quad (A.13)$$
$$a_{\mathrm{e1}}^{\mathrm{P1}}(t) = C_4 + \frac{C_3}{N_c} + C_{10} + \frac{C_9}{N_c},$$

$$a_{\mathrm{e1}}^{\mathrm{P3}}(t) = \left(C_6 + \frac{C_5}{N_c}\right) + \left(C_8 + \frac{C_7}{N_c}\right),$$

$$a_{\mathrm{e2}}^{\mathrm{T}}(t) = C_1 + \frac{C_2}{N_c}, \tag{A.14}$$

$$a_{\mathrm{e2}}^{\mathrm{P1}}(t) = -\left(C_4 + \frac{C_3}{N_c}\right) + \frac{3}{2}\left(C_9 + \frac{C_{10}}{N_c}\right) + \frac{1}{2}\left(C_{10} + \frac{C_9}{N_c}\right),$$

$$a_{\mathrm{e2}}^{\mathrm{P2}}(t) = -\frac{3}{2}\left(C_7 + \frac{C_8}{N_c}\right), \tag{A.15}$$

$$a_{\mathrm{e2}}^{\mathrm{P3}}(t) = -\left(C_6 + \frac{C_5}{N_c}\right) + \frac{1}{2}\left(C_8 + \frac{C_7}{N_c}\right).$$

All the Wilson coefficients C_i above should be evaluated at the appropriate scale t. The hard scale t is chosen as the maximum of the virtuality of the internal momentum transition in the hard amplitudes, including $1/b_i$:

$$t_{\mathrm{e}}^{(1)} = \max\left(|\alpha_{\mathrm{e}}|, |\beta_{\mathrm{e1}}|, 1/b_2\right),$$
$$t_{\mathrm{e}}^{(2)} = \max\left(|\alpha_{\mathrm{e}}|, |\beta_{\mathrm{e2}}|, 1/b_2\right),$$
$$t_{\mathrm{a}}^{(1)} = \max\left(|\beta_{\mathrm{a1}}|, 1/b_2, 1/b_3\right),$$
$$t_{\mathrm{a}}^{(1)} = \max\left(|\beta_{\mathrm{a2}}|, 1/b_2, 1/b_3\right),$$

where

$$\alpha_{\mathrm{e}}^2 = (1 - x_1 - x_2)(x_1 - r_2^2)M_{B_c}^2,$$
$$\beta_{\mathrm{e1}}^2 = [r_b^2 - x_2(1 - r_2^2)]M_{B_c}^2,$$
$$\beta_{\mathrm{e2}}^2 = (1 - x_1)(x_1 - r_2^2)M_{B_c}^2,$$
$$\alpha_{\mathrm{a}}^2 = -x_2 x_3 M_{B_c}^2(1 - r_2^2),$$
$$\beta_{\mathrm{a1}}^2 = -x_3 M_{B_c}^2(1 - r_2^2), \tag{A.16}$$
$$\beta_{\mathrm{a2}}^2 = -x_2 M_{B_c}^2(1 - r_2^2).$$

2. Contributions from non-factorizable diagrams

Different from factorizable diagrams, non-factorizable diagrams include the convolution of all three wave functions and, of course, the convolution of Sudakov factors. Their amplitudes are

$$\begin{aligned}
&M_{\mathrm{e}i}^{\mathrm{T(P1)}} \\
&= \frac{8}{N_c}\pi C_F f_B M_{B_c}^2 \int_0^1 \mathrm{d}x_2\mathrm{d}x_3 \int_0^\infty b_2\mathrm{d}b_2 b_3\mathrm{d}b_3 \\
&\quad \times\phi_D(x_2,b_2)\phi_\pi(x_3) \\
&\quad \times\Big\{\left[1 - x_1 - x_3 - (1 - x_1 - x_2)r_2 - (x_2 - 2x_3)r_2^2\right] \\
&\quad \times E_{ne\ i}^{\mathrm{T(P1)}}(t_{\mathrm{a}}^{(1)})\, H_{\mathrm{a}}(\alpha_{\mathrm{ne}}, \beta_{\mathrm{ne1}}, b_2, b_3) \\
&\quad + [(2x_1 + x_2 - x_3 - 1) + (1 - x_1 - x_2)r_2 \\
&\quad + (-2x_1 - x_2 + 2x_3)r_2^2] \\
&\quad \times E_{ne\ i}^{\mathrm{T(P1)}}(t_{\mathrm{a}}^{(2)})\, H_{\mathrm{a}}(\alpha_{\mathrm{ne}}, \beta_{\mathrm{ne2}}, b_2, b_3)\Big\},
\end{aligned} \tag{A.17}$$

$$\begin{aligned}
&M_{ei}^{\mathrm{P2}} \\
&= \frac{8}{N_c}\pi r_\pi C_F f_B M_{B_c}^2 \int_0^1 \mathrm{d}x_2\mathrm{d}x_3 \int_0^\infty b_2\mathrm{d}b_2 b_3\mathrm{d}b_3 \\
&\quad \times\phi_D(x_2,b_2) \\
&\quad \times\Big\{[(1 - x_1 - x_3 + (2 - 2x_1 - x_2 - x_3)r_2 \\
&\quad + (1 - x_1 - x_2 + x_3)r_2^2)\, \phi_\pi^p(x_3) \\
&\quad + (1 - x_1 - x_3 + (x_2 - x_3)r_2 \\
&\quad + (-1 + x_1 + x_2 + x_3)r_2^2)\, \phi_\pi^\sigma(x_3)] \\
&\quad \times E_{ne\ i}^{\mathrm{P2}}(t_{\mathrm{a}}^{(1)})\, H_{\mathrm{a}}(\alpha_{\mathrm{ne}}, \beta_{\mathrm{ne1}}, b_2, b_3) \\
&\quad + [(x_1 - x_3 + (2x_1 + x_2 - x_3 - 1)r_2 \\
&\quad + (x_1 + x_2 + x_3 - 2)r_2^2)\, \phi_\pi^p(x_3) \\
&\quad + (-x_1 + x_3 + (x_2 + x_3 - 1)r_2 \\
&\quad + (x_1 + x_2 - x_3)r_2^2)\, \phi_\pi^\sigma(x_3)] \\
&\quad \times E_{ne\ i}^{\mathrm{P2}}(t_{\mathrm{a}}^{(2)})\, H_{\mathrm{a}}(\alpha_{\mathrm{ne}}, \beta_{\mathrm{ne2}}, b_2, b_3)\Big\},
\end{aligned} \tag{A.18}$$

$$\begin{aligned}
&M_{ei}^{\mathrm{P3}} \\
&= \frac{8}{N_c}\pi C_F f_B M_{B_c}^2 \int_0^1 \mathrm{d}x_2\mathrm{d}x_3 \int_0^\infty b_2\mathrm{d}b_2 b_3\mathrm{d}b_3 \\
&\quad \times\phi_D(x_2,b_2)\phi_\pi(x_3) \\
&\quad \times\Big\{[-2 + 2x_1 + x_2 + x_3 + (1 - x_1 - x_2)r_2 \\
&\quad + (2 - 2x_1 - x_2 - 2x_3)r_2^2] \\
&\quad \times E_{ne\ i}^{\mathrm{P3}}(t_{\mathrm{a}}^{(1)})\, H_{\mathrm{a}}(\alpha_{\mathrm{ne}}, \beta_{\mathrm{ne1}}, b_2, b_3) \\
&\quad + \left[-x_1 + x_3 + (x_1 + x_2 - 1)r_2 - (x_2 + 2x_3 - 2)r_2^2\right] \\
&\quad \times E_{ne\ i}^{\mathrm{P3}}(t_{\mathrm{a}}^{(2)})\, H_{\mathrm{a}}(\alpha_{\mathrm{ne}}, \beta_{\mathrm{ne2}}, b_2, b_3)\Big\},
\end{aligned} \tag{A.19}$$

$$\begin{aligned}
&M_a^{\mathrm{T(P1)}} \\
&= \frac{8}{N_c}\pi C_F f_B M_{B_c}^2 \int_0^1 \mathrm{d}x_2\mathrm{d}x_3 \int_0^\infty b_2\mathrm{d}b_2 b_3\mathrm{d}b_3 \phi_D(x_2,b_2) \\
&\quad \times\Big\{[(-x_1 + x_2 + r_2)\phi_\pi(x_3) \\
&\quad +(-2x_1 + x_2 + x_3 + 4r_2)r_2 r_\pi \phi_\pi^p(x_3) \\
&\quad + (x_2 - x_3)r_2 r_\pi \phi_\pi^\sigma(x_3)] \\
&\quad \times E_{\mathrm{ne1}}^{\mathrm{T(P1)}}(t_{\mathrm{na}}^{(1)})\, H_{\mathrm{na}}(\alpha_{\mathrm{na}}, \beta_{\mathrm{na1}}, b_2) \\
&\quad + \left[\left(1 - x_1 - x_3 - r_b + (-x_2 + 2x_3 + r_b)r_2^2\right)\phi_\pi(x_3)\right. \\
&\quad +(2 - 2x_1 - x_2 - x_3 - 4r_b)r_2 r_\pi \phi_\pi^p(x_3) \\
&\quad + (x_2 - x_3)r_2 r_\pi \phi_\pi^\sigma(x_3)] \\
&\quad \times E_{\mathrm{ne1}}^{\mathrm{T(P1)}}(t_{\mathrm{na}}^{(2)})\, H_{\mathrm{na}}(\alpha_{\mathrm{na}}, \beta_{\mathrm{na2}}, b_2)\Big\},
\end{aligned} \tag{A.20}$$

$$
\begin{aligned}
&M_a^{\mathrm{P2}} \\
&= -\frac{8}{N_c}\pi C_F f_B M_{B_c}^2 \int_0^1 \mathrm{d}x_2 \mathrm{d}x_3 \int_0^\infty b_2 \mathrm{d}b_2 b_3 \mathrm{d}b_3 \\
&\quad \times \phi_D(x_2,b_2)\Big\{\big[(-x_1+x_2-r_2)r_2\,\phi_\pi(x_3) \\
&\quad + \big(x_1-x_3+r_2+(x_1-x_2+x_3)r_2^2\big)\,r_\pi\phi_\pi^p(x_3) \\
&\quad + \big(x_1+x_2-x_3+(-x_1+x_2+x_3)r_2^2\big)\,r_\pi\,\phi_\pi^\sigma(x_3)\big] \\
&\quad \times E_{\mathrm{ne1}}^{\mathrm{P2}}(t_{\mathrm{na}}^{(1)})\,H_{\mathrm{na}}(\alpha_{\mathrm{na}},\beta_{\mathrm{na1}},b_2) \\
&\quad - [(-1-r_b+x_1+x_2)r_2\phi_\pi(x_3) \\
&\quad + \big(1+r_b-x_1-x_3+(1+r_b-x_1-x_2+x_3)r_2^2\big) \\
&\quad \times r_\pi\,\phi_\pi^p(x_3) \\
&\quad + \big(1+r_b-x_1-x_3+(-1-r_b+x_1+x_2+x_3)r_2^2\big) \\
&\quad \times r_\pi\phi_\pi^\sigma(x_3)]\,E_{\mathrm{ne1}}^{\mathrm{P2}}(t_{\mathrm{na}}^{(2)})\,H_{\mathrm{na}}(\alpha_{\mathrm{na}},\beta_{\mathrm{na2}},b_2)\Big\}, \qquad (\mathrm{A.21})
\end{aligned}
$$

where the hard kernel H_{na} is defined as

$$H_{\mathrm{na}}(\alpha,\beta,b) = \frac{K_0(\alpha b)-K_0(\beta b)}{\beta^2-\alpha^2}, \qquad (\mathrm{A.22})$$

and the factor $E(t)$ turns into

$$E_{\mathrm{ne}j}^{\mathrm{T(P}i)}(t) = \alpha_{\mathrm{s}}(t) a_{\mathrm{ne}j}^{\mathrm{T(P}i)}(t)\,S_D(t)S_\pi(t), \qquad (\mathrm{A.23})$$

where the Wilson coefficients a read

$$
\begin{aligned}
a_{\mathrm{ne1}}^{\mathrm{T}}(t) &= C_1, \\
a_{\mathrm{ne1}}^{\mathrm{P1}}(t) &= C_3+C_9, \\
a_{\mathrm{ne1}}^{\mathrm{P2}}(t) &= C_5+C_7, \\
a_{\mathrm{ne2}}^{\mathrm{T}}(t) &= C_2, \\
a_{\mathrm{ne2}}^{\mathrm{P1}}(t) &= -C_3+\frac{1}{2}C_9+\frac{3}{2}C_{10}, \\
a_{\mathrm{ne2}}^{\mathrm{P2}}(t) &= -C_5+\frac{1}{2}C_7, \\
a_{\mathrm{ne2}}^{\mathrm{P3}}(t) &= \frac{3}{2}C_8. \qquad (\mathrm{A.24})
\end{aligned}
$$

The hard scale t is chosen as the maximum of the virtuality of the internal momentum transition in the hard amplitudes, including $1/b_i$:

$$
\begin{aligned}
t_{\mathrm{e}}^{(1)} &= \max\left(|\alpha_{\mathrm{ne}}|,|\beta_{\mathrm{ne1}}|,1/b_2,1/b_3\right), \\
t_{\mathrm{e}}^{(2)} &= \max\left(|\alpha_{\mathrm{ne}}|,|\beta_{\mathrm{ne2}}|,1/b_2,1/b_3\right), \\
t_{\mathrm{a}}^{(1)} &= \max\left(|\alpha_{\mathrm{na}}|,|\beta_{\mathrm{na1}}|,1/b_2\right), \\
t_{\mathrm{a}}^{(1)} &= \max\left(|\alpha_{\mathrm{na}}|,|\beta_{\mathrm{na2}}|,1/b_2\right),
\end{aligned}
$$

where

$$
\begin{aligned}
\alpha_{\mathrm{e}}^2 &= (1-x_1-x_2)(x_1-r_2^2)M_{B_c}^2, \\
\beta_{\mathrm{ne1}} &= -(1-x_1-x_2) \\
&\quad \times \left[(1-x_3)(1-r_2^2)-x_1+r_2^2\right]M_{B_c}^2, \\
\beta_{\mathrm{ne2}} &= -(1-x_1-x_2)\left[x_3(1-r_2^2)-x_1+r_2^2\right]M_{B_c}^2, \\
\alpha_{\mathrm{a}}^2 &= -x_2x_3M_{B_c}^2(1-r_2^2), \\
\beta_{\mathrm{na1}} &= x_1\left[x_2+x_3(1-r_2^2)\right]M_{B_c}^2, \\
\beta_{\mathrm{na1}} &= (1-x_1)\left[x_2+x_3(1-r_2^2)\right]M_{B_c}^2. \qquad (\mathrm{A.25})
\end{aligned}
$$

Appendix B: The π meson wave functions

The different distribution amplitudes of π meson wave functions are given as [15,16]

$$
\begin{aligned}
\phi_\pi(x) &= \frac{3}{\sqrt{6}}f_\pi x(1-x) \qquad (\mathrm{A.1}) \\
&\quad \times\left[1+0.44C_2^{3/2}(2x-1)+0.25C_4^{3/2}(2x-1)\right], \\
\phi_\pi^p(x) &= \frac{f_\pi}{2\sqrt{6}} \qquad (\mathrm{A.2}) \\
&\quad \times\left[1+0.43C_2^{1/2}(2x-1)+0.09C_4^{1/2}(2x-1)\right], \\
\phi_\pi^\sigma(x) &= \frac{f_\pi}{2\sqrt{6}}(1-2x)\left[1+0.55(10x^2-10x+1)\right], \qquad (\mathrm{A.3})
\end{aligned}
$$

with the Gegenbauer polynomials

$$
\begin{aligned}
C_2^{1/2}(t) &= \frac{1}{2}(3t^2-1), \quad C_4^{1/2}(t) = \frac{1}{8}(35t^4-30t^2+3), \\
C_2^{3/2}(t) &= \frac{3}{2}(5t^2-1), \quad C_4^{3/2}(t) = \frac{15}{8}(21t^4-14t^2+1). \qquad (\mathrm{A.4})
\end{aligned}
$$

References

1. CDF Collaboration, F. Abe et al., Phys. Rev. D **58**, 112004 (1998)
2. Y.Y. Keum, H.N. Li, A.I. Sanda, Phys. Rev. D **63**, 054008 (2001); C.H. Chen, Y.Y. Keum, H. n. Li, Phys. Rev. D **64**, 112002 (2001); Y.Y. Charng, H. n. Li, hep-ph/0308257
3. C.-D. Lü, K. Ukai, M.-Z. Yang, Phys. Rev. D **63**, 074009 (2001); C.-D. Lü, p. 173–184, Proceedings of International Conference on Flavor Physics (ICFP 2001) (World Scientific, 2001), hep-ph/0110327
4. M. Beneke, G. Buchalla, M. Neubert, C.T. Sachrajda, Phys. Rev. Lett. **83**, 1914 (1999); Nucl. Phys. B **606**, 245 (2001); M. Beneke, M. Neubert, Nucl. Phys. B **675**, 333 (2003)
5. C.W. Bauer, D. Pirjol, I.W. Stewart, Phys. Rev. Lett. **87**, 201806 (2001); Phys. Rev. D **65**, 054022 (2002); C.W. Bauer, I.W. Stewart, Phys. Lett. B **516**, 134 (2001); B **516**, 134 (2001); Phys. Rev. D **65**, 054022 (2002)
6. D. Du, Z. Wang, Phys. Rev. D **39**, 1342 (1989)
7. J. Schwinger, Phys. Rev. Lett. **12**, 630 (1965); M. Bauer, B. Stech, Phys. Lett. B **152**, 380 (1985); M. Bauer, B. Stech, M. Wirbel, Z. Phys. C **34**, 103 (1987)
8. A. Ali, C. Greub, Phys. Rev. D **57**, 2996 (1998); A. Ali, J. Chay, C. Greub, P. Ko, Phys. Lett. B **424**, 161 (1998);

A. Ali, G. Kramer, C.D. Lü, Phys. Rev. D **58**, 094009 (1998); Y.-H. Chen, H.-Y. Cheng, B. Tseng, K.-C. Yang, Phys. Rev. D **60**, 094014 (1999)
9. T. Kurimoto, H.-n. Li, A.I. Sanda, Phys. Rev. D **67**, 054028 (2003)
10. C.D. Lü, M.Z. Yang, Eur. Phys. J. C **28**, 515 (2003)
11. G. Buchalla, A.J. Buras, M.E. Lautenbacher, Rev. Mod. Phys. **68**, 1125 (1996)
12. J.F. Liu, K.T. Chao, Phys. Rev. D **56**, 4133 (1997); C.Q. Geng, C.W. Hwang, C.C. Liu, Phys. Rev. D **65**, 094037 (2002)
13. Y.-Y. Keum, T. Kurimoto, H.-N. Li, C.-D. Lü, A.I. Sanda, Phys. Rev. D **69**, 094018 (2004)
14. G.-L. Song, C.-D. Lü, Phys. Rev. D **70**, 034006 (2004)
15. P. Ball, JHEP **09**, 005 (1998); JHEP **01**, 010 (1999)
16. P. Ball, V.M. Braun, Y. Koike, K. Tanaka, Nucl. Phys. B **529**, 323 (1998); P. Ball, V.M. Braun, hep-ph/9808229
17. C.-H. Chang, Y.Q. Chen, Phys. Rev. D **49**, 3399 (1994)
18. Particle Data Group, Phys. Rev. D **66**, Part I (2002)
19. H.-n. Li, S. Mishima, A.I. Sanda, hep-ph/0508041
20. H.n. Li, Phys. Rev. D **66**, 094010 (2002)
21. H.-n. Li, B. Melic, Eur. Phys. J. C **11**, 695 (1999)